Regular article

Inhomogeneous reduction and its relation to grain growth of titania during flash sintering

Harry Charalambous [a],*, Shikhar Krishn Jha [a], Han Wang [b], Xin Li Phuah [b], Haiyan Wang [b], Thomas Tsakalakos [a]

[a] Department of Materials Science and Engineering, Rutgers University, 607 Taylor Road, Piscataway, NJ 08854, United States
[b] School of Materials Engineering, Purdue University, Neil Armstrong Hall of Engineering, 701 West Stadium Avenue, West Lafayette, IN 47907, United States

ARTICLE INFO

ABSTRACT

Flash sintering under DC electric field partially reduces titania (rutile) and promotes abnormal grain growth near the anode. The resulting reduction in grain boundary density reduces the number of vacancy traps and enhances the O^{2-} ion conductivity through the specimen, facilitating greater non-stoichiometry. The observed gradient of densification and grain-growth across the two ends has been linked to the Peltier effect which causes heating at the anode-electrode junction and cooling at the cathode-electrode junction.

Published by Elsevier Ltd on behalf of Acta Materialia Inc.

Flash sintering (FS) utilizes an electric field, which is applied across a ceramic green body at high temperature and results in a non-linear rise in current through the sample, causing rapid densification. Flash sintering was first shown to reduce the required furnace temperature for sintering of 3 mol% yttria-stabilized zirconia (3YSZ) from 1450 °C for conventional sintering (CS) to 850 °C and additionally lowered the time to under 5 s [1].

Despite the work of many researchers there is still a great deal of debate as to the predominant mechanism responsible for the enhanced diffusion during the flash event. Three proposed mechanisms include rapid heating and the resulting destabilization of the grain boundaries [2, 3], an avalanche of Frenkel pair defects induced by the electric field which enhances the diffusion pre-exponential factor [1, 4–7], and local melting or softening of the grain boundaries due to inhomogeneous temperature distribution, which enhances diffusion across the grain boundaries [8, 9].

In ionic and mixed electronic-ionic conductors diffusion through vacancy and interstitial mechanisms takes place under the influence of a chemical potential. The observation of defects in the bulk during or post flash has been claimed as evidence that Frenkel pairs are generated and enhance the kinetics of sintering [6, 10]. However, diffusion of oxygen vacancy-interstitial pairs alone does not lead to densification as diffusion of both the species are required.

For the case of titania, found in three polymorphs (rutile, anatase, and brooktite), rutile is the only stable phase at high temperatures

and is a mixed conductor. Rutile and composites containing rutile is a common model system studied in flash sintering works [11–17].

Although in situ flash sintering of TiO_2 [17] as well as ZnO [18] and 3YSZ [10] give direct evidence of oxygen diffusion during flash sintering, detection of oxygen vacancies post-flash sintering has been elusive due to the relatively slow cooling of the furnace which allows enough time for the non-equilibrium defects, namely interstitials and vacancies, to annihilate. In addition, the high surface area to volume ratio of a dogbone design allows for rapid re-oxidation. In contrast, experiments with thicker cylindrical pellets and rapid furnace cooling allow analysis of the reduction of titania, $TiO_2 \rightarrow xV_O^{\bullet\bullet} + TiO_{2-x}$. This reduction is clearly observed through blackening of the TiO_2 pellet interior unlike in previous studies of flash sintering of ZnO [19, 20], a related n-type semiconductor.

Inhomogeneity in the microstructure across the electrodes has been discussed in detail in a review by Yu et al. [21]. Other chemical inhomogeneity observations during flash sintering have been made. For example, blackening at the cathode of tricalcium phosphate (TCP) [22] was attributed to oxidation at the anode and reduction at the cathode. Also, a buildup of magnesium near the cathode in magnesia-silicate glass-containing alumina [23, 24] and sodium in soda lime silicate glass [25] was caused by migration of positively charged ions towards the cathode. Preferential non-stoichiometry across the specimen length was also shown by Jha et al. for the case of ceria [26]. In this case the measurements were taken in situ and show a peak splitting which indicates reduction of ceria at the cathode.

Raman spectroscopy and X-ray photoelectron spectroscopy (XPS) were used to study the chemistry and crystallinity across the FS

---

* Corresponding author.
  E-mail address: harry.charalambous@rutgers.edu (H. Charalambous).

specimen. These tools were used to map inhomogeneity in the reduction which had a greater concentration at the anode. Analysis of the microstructure indicated a distinct electrode effect in sintering, with more intergranular porosity and less grain growth at the cathode and intragranular porosity and rapid grain growth at the anode.

Rutile titania nanopowder, grain size ~50 nm, was acquired from Inframat Advanced Materials, Product # 22N-0814R. The powder was loaded into a 6 mm die with uniaxial, 200 MPa applied pressure, which achieved a green body density of ~52%.

For FS, samples were coated with platinum paste on both faces and placed inside a cylindrical, alumina stage with platinum electrodes in contact at both ends. The specimens were then heated at a rate of 10 °C/min under 50 V/cm DC electric field applied at 500 °C. The alumina stage was placed inside an alumina tube enclosure within the furnace, which created a depleted oxygen atmosphere where oxygen could not be easily replenished and initiated the runaway effect of flash with a significantly lower electric field than mentioned in the literature [11].

As the sample was heated it became more conductive, which allowed a small current flow. The internal resistance to the current heated the sample and allowed even more current to flow. The external, conductive heating due to the ramp of the furnace and the internal, resistive heating of the sample due to current flow created a feedback loop that resulted in a rise in current and rapid densification. To avoid runaway heating a limit was placed on the current, in this case 5 A/cm^2, and the electric field dropped accordingly. This stage was held for 1 min before the electric field was turned off altogether and the furnace was cooled at a rate of 25 °C/min.

A comparison was made using a CS specimen at 1150 °C with heating rate of 10 °C/min, 1 min hold time, and cooling rate of 25 °C/min. Both specimens were cut vertically to expose the cross-section area from cathode to anode and were mechanically polished down to 0.25 μm using diamond polishing paste.

The specimen crystallinity was analyzed using Renishaw InVia Raman MicroSpectroscopy with spot size ~1 μm and Raman shift range 100–700 cm^{-1}. Three spots were mapped: the cathode and anode for the FS sample, and middle for the CS standard. The specimen chemistry was analyzed using ThermoFisher K-Alpha X-Ray Photoelectron Spectroscopy (XPS) with 1486.7 keV x-ray photon energy and 400 μm spot size. Three spots were mapped at different sections of the cross-section area: cathode, middle, and anode. After completion of a survey scan over a binding energy range from 1350 eV–0 eV with 1 eV step size, the specific regions 298 eV–279 eV (C1s), 475 eV–448 eV (Ti2p), and 545 eV–525 eV (O1s) were scanned in detail (see Supplementary Fig. S1) for each position.

After completion of analysis with Raman Spectroscopy and XPS, the samples were both thermally etched at 900 °C for 1 h to reveal the grain boundaries for the SEM micrographs. The samples were coated with 10 nm of gold and a Zeiss Sigma Field Emission SEM with 5 kV electron gun was used to characterize the microstructures. Separately, a FS specimen under the same conditions was prepared for imaging under transmission electron microscopy (TEM). The sample was sectioned to create plan-view samples of the cathode, middle and anode. Each section was ground, polished and dimpled, followed by final polishing done using a precision ion milling machine, PIPS II, Gatan. Microstructural characterization was completed by the FEI TALOS F200X TEM operated at 200 kV.

The three stages of flash sintering [27] are shown in Fig. 1. In stage I, the sample temperature rise high enough for necking to occur between grains. The necking creates conduction paths for a small current, which results in modest dimensional shrinkage. As a constant voltage is applied to the shrinking sample, the apparent electric field increases and, combined with increased conductivity due to densification and heating, an exponential rise in current necessitates a current limit to avoid thermal runaway. This stage is where most of the densification occurs along with pore closure [12]. In the final stage of flash sintering the electric field gradually declines to a steady state to maintain constant current. Final densification and grain growth are characteristic of this stage.
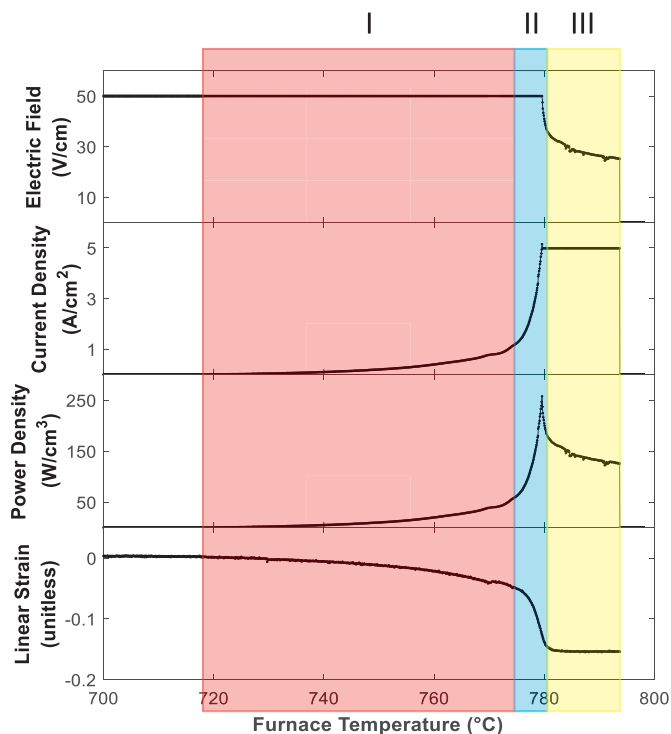

Fig. 1. An electric field is applied as TiO$_2$ is heated resulting in a nonlinear rise in current which is limited to a maximum value of 5 A/cm^2 by limiting the applied electric field. The resulting power density (P = EJ) causes rapid densification, represented by linear strain. The three stages of flash (I, II, and III) are labelled. While most of the densification occurs in stage II, grain growth continues in stage III.

With significant grain growth pore breakaway occurs, resulting in round intragranular pores [28].

The microstructure, indicated in Fig. 2, shows three distinct regions. At the cathode, Fig. 2(a) and (d), pore closure is incomplete and grain growth is limited (0.41 ± 0.15 μm). In the middle region, Fig. 2(b) and (e), most pores have been eliminated and gradual grain growth (0.90 ± 0.43 μm) occurs, indicated by limited intragranular porosity. Large grains (1.34 ± 0.66 μm), intragranular porosity, and regions of abnormal grain growth are evident at the anode, Fig. 2(c) and (f). A summary of these results and comparison to conventional sintering is given in Supplementary Fig. S2.

A vertical cross section of the pellet is shown in Fig. 3(a) with cathode, middle, and anode corresponding to white, grey, and dark grey coloration. Three fundamental Raman vibration modes are identified for rutile: B$_{1g}$ = 144 cm^{-1} O—Ti—O bending mode, E$_g$ = 448 cm^{-1} O c-axis liberation mode, and A$_{1g}$ = 612 cm^{-1} Ti—O stretch mode [29–31]. Comparison of the cathode, anode, and CS reference indicates no visible Raman peak shift for the three identified fundamental Raman modes, Fig. 3(b). However, Raman peak reduction and broadening (Fig. 3(c)), especially at the anode, indicates a decrease in crystallinity [32–34] which is counterintuitive considering the increase in grain size and corresponding reduction in the number of grain boundaries.

XPS analysis of three positions corresponding to measurements from cathode to middle to anode indicates a downshift of the binding energies for the Ti2p$_{3/2}$ (458.9 eV to 458.7 eV), Ti2p$_{1/2}$ (464.6 eV to 464.4 eV), and O1s metal oxide bonds (530.2 eV to 530.1 eV), shown in Fig. 3(d) and (e). A small shift in the binding energies of the core Ti2p$_{3/2}$ and Ti2p$_{1/2}$ (0.2 eV) electrons is significant as the effect of an extra electron in the valance band will be dampened due to electron shielding. Small XPS downshift, corresponding to reduction of a portion of Ti^{4+} ions to Ti^{3+}, indicates an increase of $V_O^{\bullet\bullet}$ defects in agreement with other studies [35, 36].

Three possible explanations are provided for the gradient of oxygen vacancies corresponding with enhanced sintering and grain growth: